PROCEEDINGS OF SPIE

SPIEDigitalLibrary.org/conference-proceedings-of-spie

The large fiber array spectroscopic telescope: opto-mechanical design and architecture

Andrew Young, Roger Angel, Chad Bender, Joel Berkson, Peter Gray, et al.

Andrew J Young, Roger Angel, Chad Bender, Joel Berkson, Peter Gray, Samuel Halverson, Hyukmo Kang, Daewook Kim, Andy Monson, Chang-Jin Oh, Matthew Rademacher, Christian Schwab, Dennis Zaritsky, "The large fiber array spectroscopic telescope: opto-mechanical design and architecture," Proc. SPIE 12182, Ground-based and Airborne Telescopes IX, 121824B (26 August 2022); doi: 10.1117/12.2629330

SPIE.

Event: SPIE Astronomical Telescopes + Instrumentation, 2022, Montréal, Québec, Canada

The Large Fiber Array Spectroscopic Telescope: Opto-Mechanical Design and Architecture

Andrew Young[b], Roger Angel[a], Chad Bender[a], Joel Berkson[b], Peter Gray[a], Samuel Halverson[c], Hyukmo Kang[b], Daewook Kim[a,b], Andy Monson[a], Chang-Jin Oh[b], Matthew Rademacher[a], Christian Schwab[d], Dennis Zaritsky[a]

[a]Department of Astronomy and Steward Observatory, University of Arizona, 933 N. Cherry Ave., Tucson, AZ 85721, USA
[b]Wyant College of Optical Sciences, University of Arizona, 1630 E. University Blvd., Tucson, AZ 85721, USA
[c]Jet Propulsion Laboratory, California Institute of Technology, Pasadena, CA 91109, USA
[d]Department of Physics and Astronomy, Macquarie University, North Ryde, NSW 2109 Australia

ABSTRACT

This paper describes the preliminary mechanical design and optomechanics of LFAST, the Large Fiber Array Spectroscopic Telescope. The 1,200 m^2 array comprises 132, open air, alt-az tracking mounts, each carrying 20 small co-aligned telescopes in a 5 m square U-shaped space frame about a central, dual-axis worm drive. Each unit telescope has a 0.76 m, f/3.5 mirror, a prime focus assembly with field corrector and a guide camera, and feeds a 17um, 1.3 arcsecond optical fiber. LFAST was designed specifically as a fiber fed spectroscopic telescope. By being built from thousands of mass-produced components it will be much cheaper per square meter of collecting area than phased monolithic telescopes currently under construction, like GMT and ELT. Cost effective dome-less operation is made possible by the structural design that maximizes stiffness and active compensation for wind induced jitter. The primary mirrors are protected when not in use by sub-horizon pointing of tracking mount and mirror covers.

Keywords: LFAST, Optomechanical Design, Array Telescope, Passive Support, Whiffle Tree

1. INTRODUCTION AND OVERVIEW

The Large Fiber Array Spectroscopic Telescope (LFAST) is an open-air optical telescope array comprised of 132 dual axis tracking mounts each carrying 20 individual, coaligned, 0.76 m unit telescopes, each feeding a 17 um (1.3 arcsec) fiber taking light to a high-resolution spectrograph [1,2]. LFAST is designed to provide a very large aperture (1200 m^2) at low cost and will be dedicated to spectroscopic observations. The tracking mounts, shown in Figure 1, use steel space frames to carry the individual primary mirrors and prime focus correctors using central pier-mounted azimuth and elevation worm drives mass produced for the solar tracker industry. Precise co-alignment and gravitational flexure compensation of the 20 unit telescopes on the tracking mount will be achieved with active tip tilt control of the meniscus primary mirrors. The tracking mount frame has been designed to be stiff enough that active tip tilt control to correct differential misalignment of the prime focus correctors is not required to maintain sharp images. Stabilization against image jitter will be obtained through rapid translation of a lens element in the prime focus corrector. Motion of the space frame and of the unit telescopes is captured by individual guide cameras, imaging the prime foci with a relay, and with inertial sensors on the tracking mount. These systems will be used in closed loop to control mount tracking and active image stabilization working to keep star images on the optical fibers when subject to wind, tracking errors, and gravitation flexure of the tracking mount.

This paper summarizes the optomechanical design of the LFAST tracking mounts and unit telescopes. The tracking mount was developed with the aid of finite element analysis to model its deformations under gravity. Using the optical model of the unit telescope in conjunction with the data from finite element analysis, we calculate star image motion and alignment induced aberrations as the mount slews in elevation to validate its performance.

A. Y.: E-mail: andrewjyoung@arizona.edu, Telephone: +1-802-355-3382

Ground-based and Airborne Telescopes IX, edited by Heather K. Marshall, Jason Spyromilio, Tomonori Usuda,
Proc. of SPIE Vol. 12182, 121824B · © 2022 SPIE · 0277-786X
doi: 10.1117/12.2629330

Additionally, we make predictions of the wind induced excitation amplitude of the tracking mount by scaling the performance of the Atacama Large Millimeter Array (ALMA) prototype antennas [3], which are also on open-air mounts and have similar resonant frequencies. Finally, we discuss the optimization of the primary mirror whiffle tree supports to minimize rms surface error with more discussion on lateral support supplied through centrally positioned spherical bearings. On the basis of these analyses LFAST will build its first mount with 20 unit telescopes, and measure how efficiently they achieve the targeted sub-arcsecond imaging performance, as well as calculate the costs associated with each mechanical system built in high volume.

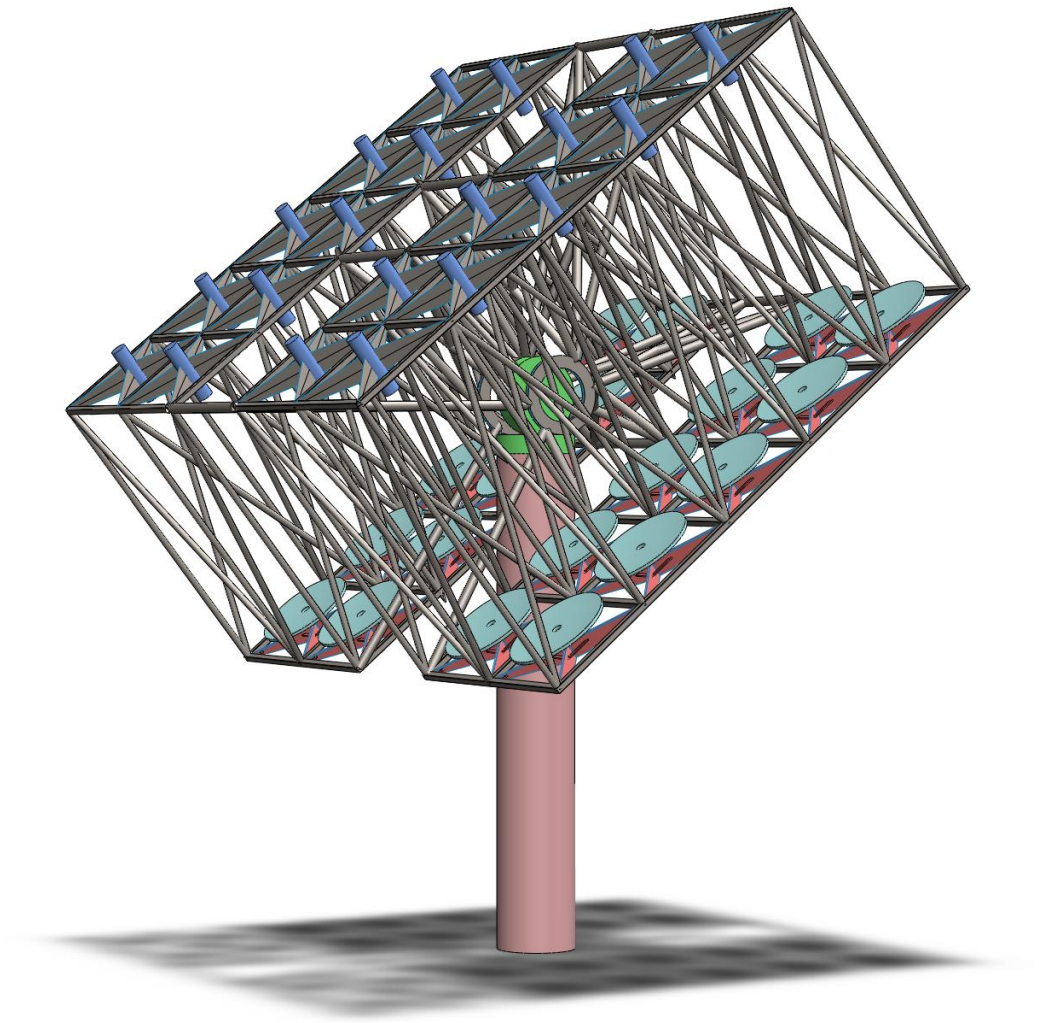

Figure 1: Isometric view of the LFAST tracking mount.

2. TRACKING MOUNT DESIGN AND PERFORMANCE

Shown in Figure 1, the tracking mount is composed of a central steel pier, a dual axis slewing drive and a steel space frame which supports all 20 unit telescopes. In lieu of a dome we designed this mount to point to 20 degrees below the horizon and incorporate deployable covers to protect the primary mirrors during the daytime. The unit telescopes are sensitive to alignment of the individual prime focus correctors to their respective primary mirrors, and all 20 unit telescopes to each other. The supporting space frame needs to maintain these alignments to about an arcminute, to control aberrations when

image positions are stabilized by active tip/tilt of the primary mirrors. Additionally, direct wind exposure is expected to excite low order modes resulting in image jitter. To reduce these vibration amplitudes to the actively correctable ~1 arc second level, using a rapidly translating lens element in the prime focus corrector described by Berkson et al [4], we designed the space frame to have high torsional stiffness and low rotational inertia about the drive altitude and azimuth axes. It is also desirable to facilitate quick maintenance on optical components in the planned array of 2640 unit telescopes, and for that we designed simple removable subframes for the primary mirror cells and spider assemblies for the prime focus correctors.

2.1 Design

Because the unit telescopes do not share a single, central focus, the space frame has been arranged to distribute the unit telescopes into two 2x5 rectangular grids symmetric about the central slewing drive, packaging the 20 apertures into a frame of approximately 4.8 x 4.8 meters. This allows for LFAST to use central inexpensive alt-az slewing drives mass-produced for industry, including for solar trackers, as opposed to the large yolk style mounts with custom drives commonly seen on large telescopes. Principal views of the LFAST space frame are shown in Figure 2 with a numbering scheme provided for the 20 unit telescopes. The vertex separation between the primary mirrors and prime focus correctors sets the depth of the space frame to approximately 3 meters accommodating the F/3.5 primaries. Future optimization of this design will look at sizing the modular components of the space frame to fit in standard shipping containers.

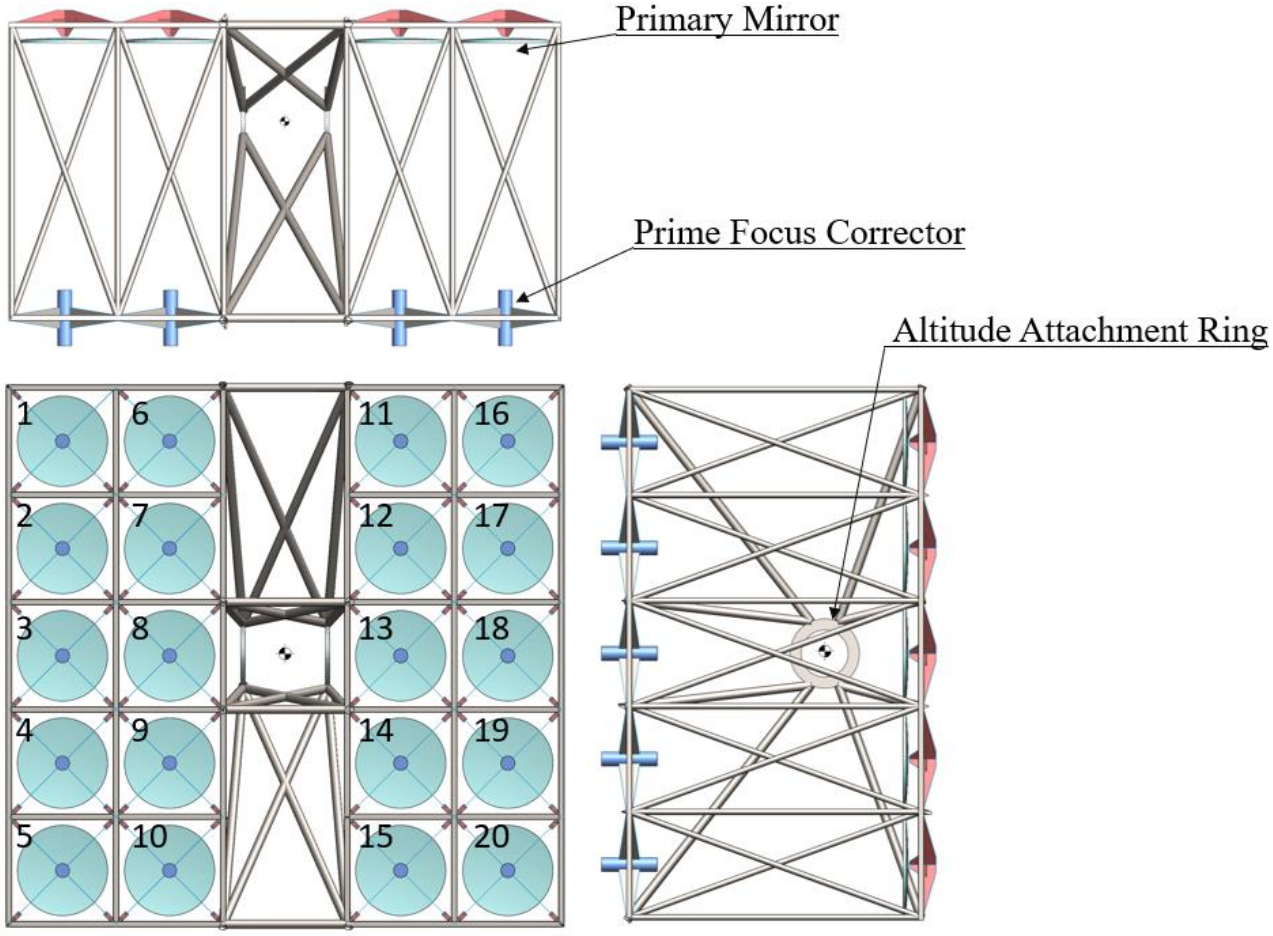

Figure 2: Top Left: Plan view of the space frame. Bottom Left: Elevation view of space frame looking down the optical axis with the unit telescope numbering scheme for reference. Bottom Right: Plan view of the space frame looking down the altitude axis.

The struts used in the design are thin walled hollow steel structual tubing with a total steel weight of 1.5 tons and a rotational inertia about the altitude axis of 8650 kg m^2. The space frame was designed with its center of mass concident with the elevation axis to achieve a neutral balance and uses altitude and azimuth bearings with dual worm drives to increase stiffness and minimize backlash. The layout of struts, drawing from the truss design of the Multiple Mirror Telescope, rigidly couples the motion of the primary mirrors and prime focus correctors for each unit telescope. Larger struts connect the two halves of the strucutre to attachment rings which bolt directly to the altitude axis of the slewing drive. The layout of these larger central struts provides torsional stiffness, supressing low order modes about the altitude axis, and gives adequate clearance around the central pier to obtain the desired range of motion highlighted in Figure 3.

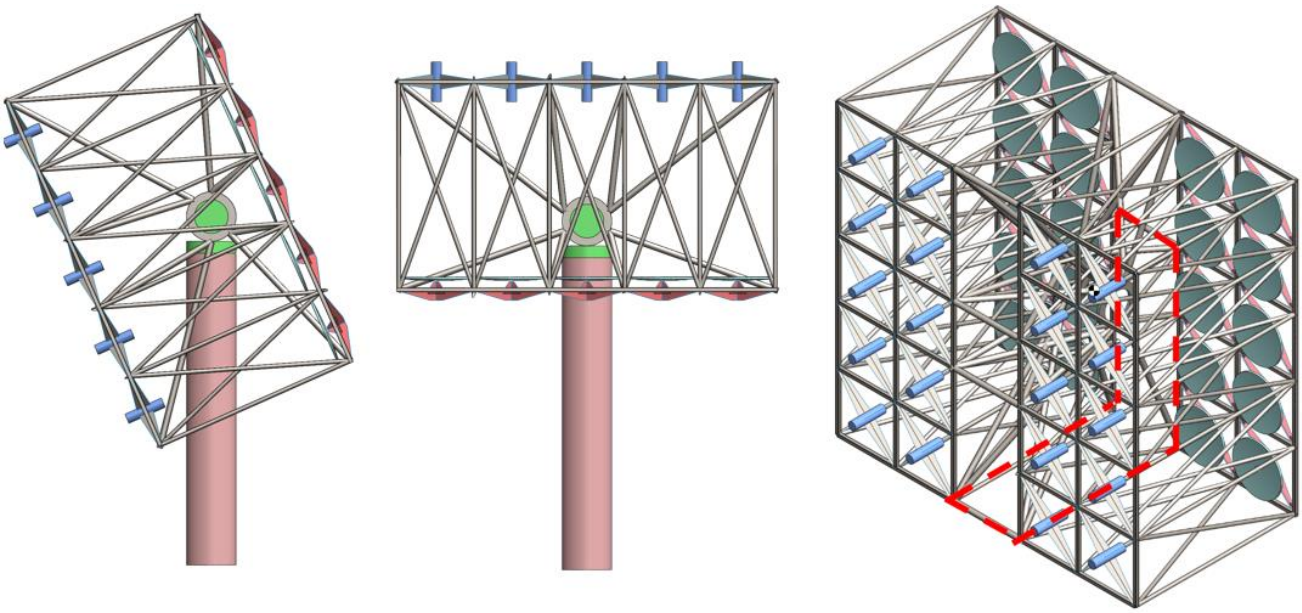

Figure 3: Left: LFAST in stowed position, pointing 20 degrees below the horizon. Middle: LFAST pointing to Zenith. Right: Red dashed lines indicate region with no structural members, so to not restrict pier motion.

Each unit telescope has two subassemblies to carry the prime focus correctors and the primary mirrors. The upper prime focus assemblies attach to the tracking mount using traditional spiders made from tensioned radial vanes. The lower primary mirrors attach to the space frame with aluminum subframes that bolt up to the back of the space frame for easy removal. An 18-point whiffletree attaches to each subframe at 3 locations with linear actuators to tip, tilt, and piston the primary mirrors. Translational degrees of freedom perpendicular to the optical axis are not required for this design as the primaries are spherical. These actuators are used to correct relative misalignments due to flexure as well as in the correction of atmospheric dispersion and defocus due to thermal expansion. To measure individual orientations, each of the unit telescopes is equipped with a guide camera working in closed loop with the primary mirror actuators. Additional feedback is provided with inertial sensors on the fame to capture the rapid dynamic wind-jitter motion of the space frame.

2.2 Finite Element Modeling

The tracking mount space frame is modeled in finite element using beam and shell elements. These elements are modeled as continuous, with adjacent nodes of beams and shells merged. The primary mirror and prime focus corrector components were modeled as discrete masses and were attached to nodes in the model corresponding to optical mounting locations on the space frame. Views of the finite element model are shown in Figure 4.

For static modeling of the gravitational flexure, the pier and slewing bearing deformations were ignored, and the space frame was fixed to ground at the altitude axis mounting rings. For the modal analysis, the stiffness and mass of both the pier and slewing drive were modeled, with the pier fixed to ground at its base. No loads or prestresses were imposed on the modal analysis model.

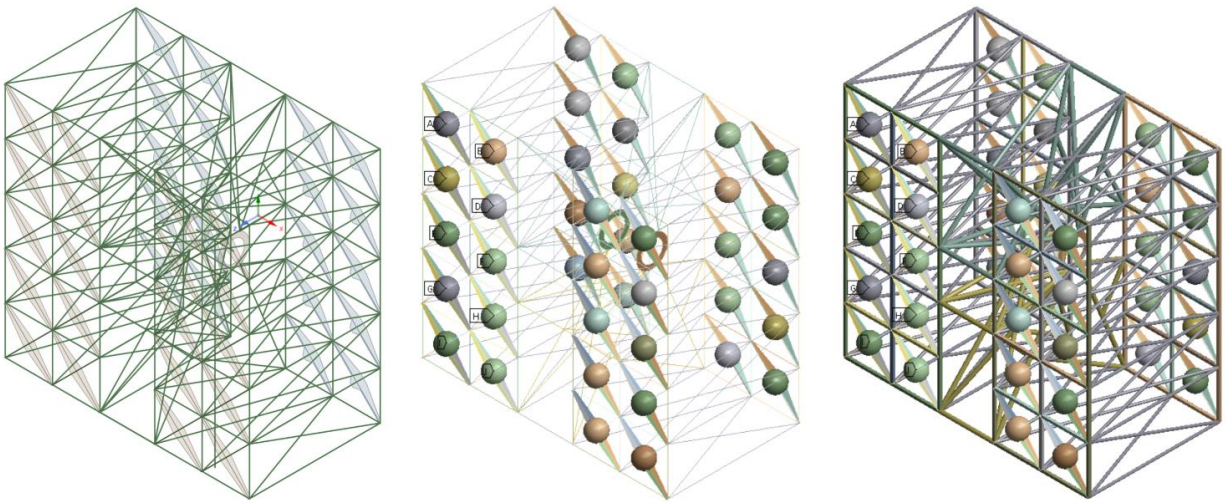

Figure 4: Left: Wireframe and surface model of the space frame. Middle: Beam and shell element model of the space frame with lumped masses providing the weight of the optics. Right: Completed model of space frame with beam and shell thicknesses rendered.

2.3 Static Analysis of Tracking Mount

Static analysis of the tracking mount under gravity yields two main results of interest. Firstly, how much image motion prior to correction, results from flexure of the space frame for each unit telescope. Secondly, how flexure-induced misalignments of the primary mirrors and prime focus correctors impact the quality of the star image. The imaging performance for each unit telescope is quantified by measuring the decrease of encircled energy at the 17um optical fiber resulting from misalignments due to flexure. To accomplish this, the flexure induced motion of the primary mirrors and prime focus correctors are calculated from the finite element model. Figure 5 shows the nodes in the model which correspond to attachment points for the primary mirrors and prime focus correctors. These nodes were used to calculate the rigid body motion of the optics by constructing centroids and orientation vectors for each optical component in each step in the analyses.

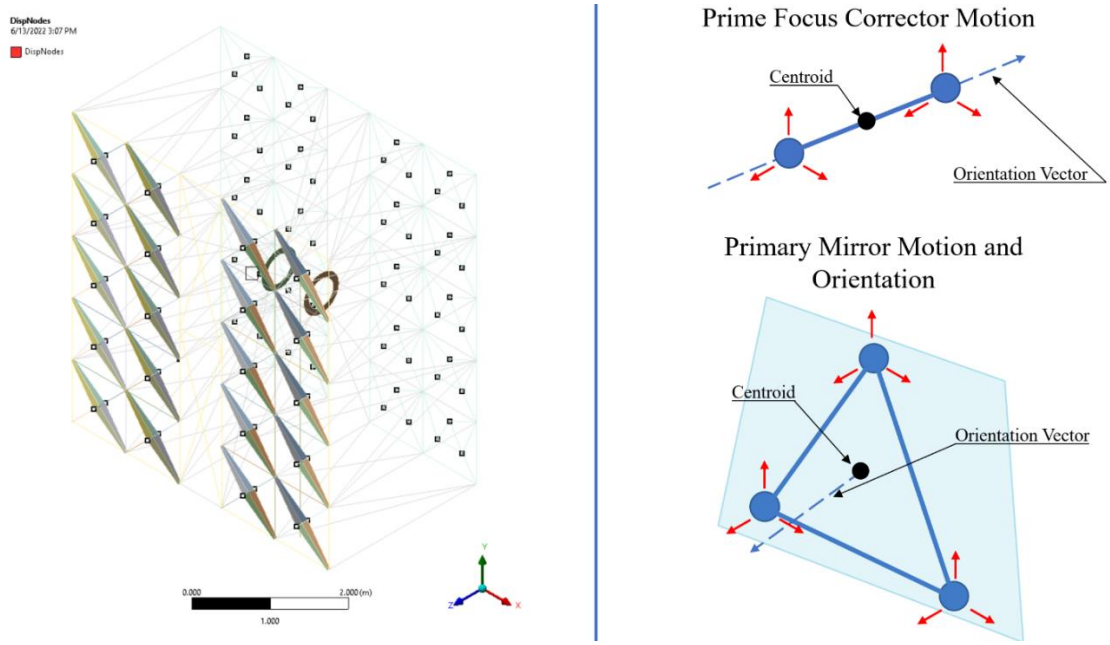

Figure 5: Left: Nodes in the finite element model which are exported for postprocessing. Right: The methods used to find the position and orientation of the prime focus correctors and primary mirrors given the node data. The centroids and orientation vectors calculated from the nodes, shown in blue, are used to model the motion of the optical elements on the space frame resulting from flexure.

Once the positions and orientations of the optical components are known relative to the optical axis, this data is fed into the optical model of the telescope to calculate both the image motion and decrease in encircled energy. To monitor this effect more efficiently for each telescope, a function was generated in the optical model to map the decrease in encircled energy resulting from rigid body motions of the optical components. Figure 6 shows the relationship between tilt of the prime focus corrector and diffraction encircled energy at 17um with polychromatic light from 380nm to 1700nm. To arrive at this plot, the prime focus corrector was tilted about its center of mass in the optical model. The primary mirror was then tilted to move the star image back onto the optical fiber and the diffraction encircled energy was measured. This was performed for various tilt angles of the prime focus corrector up to 6 arcminutes. With this, the tip/tilt of the prime focus correctors resulting from flexure was interpolated to obtain the curve shown. Because we use a spherical primary mirror, decenter of the optical components, when corrected for by tilting the primary mirror, does not aberrate the image and maintains nominal performance.

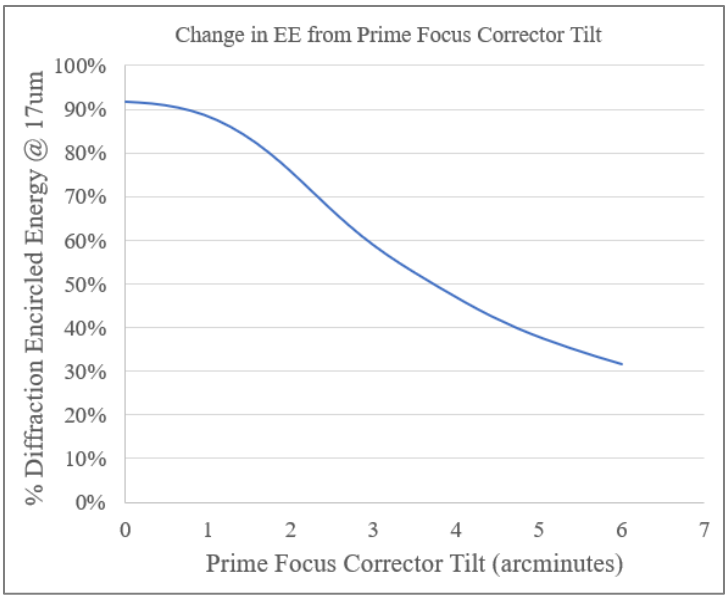

Figure 6: Decrease of diffraction encircled energy at 17um resulting from prime focus corrector tilt.

Through this analysis we characterized the unit telescopes sensitivity to prime focus corrector tilt and observed that the prime focus corrector's orientation relative to the common mount optical axis should be maintained to better than 1 arcminute. This limits encircled energy loss to less than 2% and for this reason, the space frame was designed to minimize differential motion. The current space frame maintains the alignment of the prime focus correctors to better than ~0.7 arcminutes.

Given that the deformation of the space frame varies with its altitude angle, it is advantageous to align the optical systems on the structure at an altitude where it will be doing a majority of its observing. For this analysis of the space frame, the alignment altitude is chosen to be 51 degrees, as it was the nearest step in the finite element model to 45 degrees. At this alignment altitude, the telescope is modeled as nominal with all 20 telescope axes co-aligned. Slewing away to different altitudes deforms the frame to produce alignment indued aberrations and image motion for each unit telescope on the space frame.

A simple approach to plot the star image motion resulting from deformations in the space frame used the optical model to make relationships between the rigid body motion of the optics and the star image motion. Once these relationships were found for the unit telescope, the calculated motion from finite element can be used to determine the stage image motion for every telescope on the space frame. The effect of prime focus corrector tip/tilt on star image motion was found to be fairly linear over a few degrees as was the case with primary mirror tip/tilt of the and relative decenter of both the primary mirror and prime focus corrector. These image motion relations are provided in Table 1.

Table 1: Correlations between star image motion and the motion of the unit telescope components.

Optical Element Motion	**Resulting Star Image Motion Relation**
1 micron of decenter between prime focus corrector and primary mirror.	1 micron of image motion
1 arcminute of prime focus corrector tilt	83.3 microns of image motion
1 arcminute of primary mirror tilt	~1.5 millimeters of image motion

The tilt from the primary mirror yields the greatest source of image motion and will require precise control from the primary mirror actuators. Actuator steps of 0.05um are desired to achieve an increment of 0.2 arcseconds. Linear actuators with step sizes of 0.1 microns, with correction increments of 0.4 arcseconds are currently being evaluated.

2.4 Results from Static Analysis

Figure 7 shows the change in encircled energy resulting from gravitational flexure of the tracking mount for half of the unit telescopes. Only half of the telescopes are plotted due to the symmetry of the deformations about the central slewing drive. As was done for Figure 6, to obtain this plot, the prime focus correctors were tilted for given altitude by the amount determined by finite element analysis. The primary mirrors were then tilted to move the star images back onto the optical fibers and the diffraction encircled energy for each unit telescope was calculated.

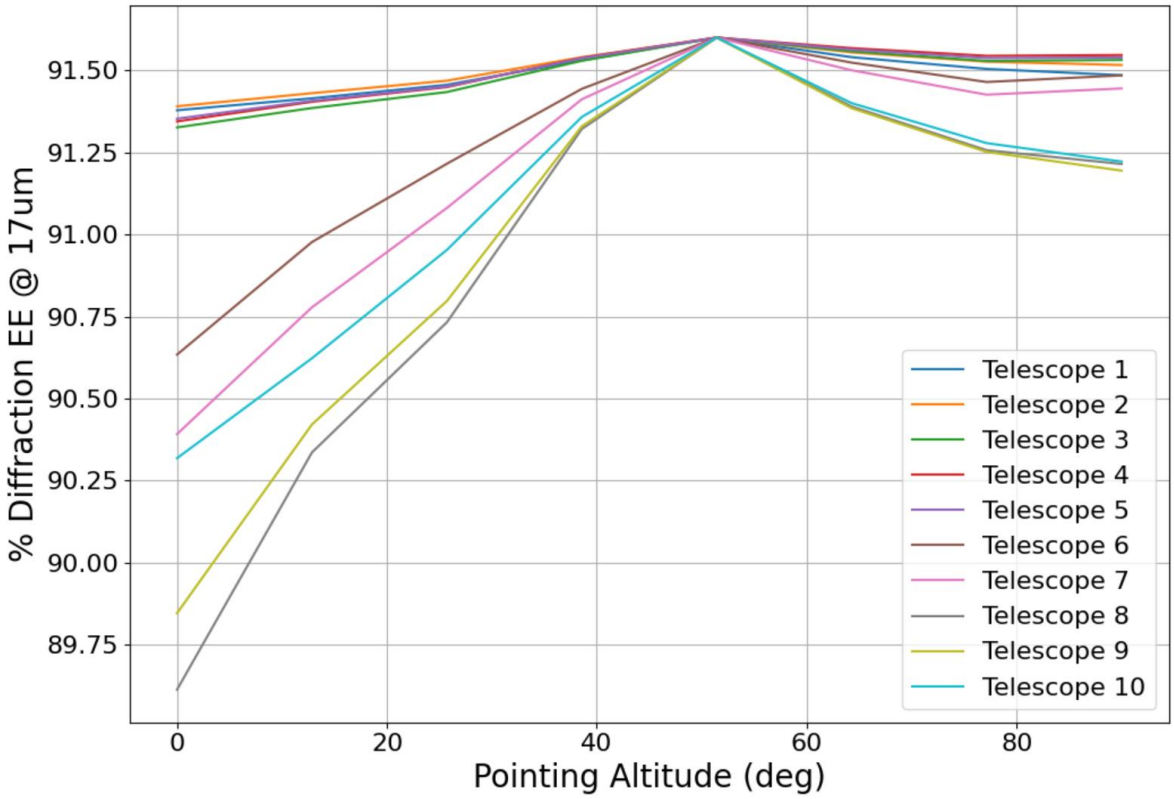

Figure 7: Change in encircled energy at the 17um optical fibers due to slewing in elevation from horizon to zenith for one half of the unit telescopes.

With the telescope aligned at 51 degrees to the horizon, and all telescopes well aligned, the encircled energy fraction is 91.6%, the 8.4% loss being from residual optical aberrations and diffraction. The maximum effect of alignment induced aberrations when pointing up in altitude to 90 degrees (zenith) is to reduce the encircled energy by 0.45% shown by telescope 9. When pointing down in altitude from 51 degrees to 10 degrees the maximum decrease of encircled energy is 1.38%, shown by telescope 8. From an altitude range of 30 – 90 degrees all unit telescopes will see a reduction in encircled energy of no greater than 0.63% largely maintaining their nominal performance. It is important to note that the active primary mirror is requisite for this performance, as the star images will drift off the fibers without tip and tilt correction.

The star image motions, prior to correction, due to changing gravitational flexure of the space frame are shown in Figure 8 for each unit telescope. Unit telescopes 7,8,12 and 13 have the largest image motion which are caused from local

deformations when pointing near zenith. Image motion due to decenter and tilt of the prime focus corrector make up less than 1% of the total. Primary mirror tilts due to flexure are less than 1 arcminute, requiring tip/tilt actuator throws of no more than ~60um to correct. This actuator range is small and easily achieved by a broad range of available linear actuators. Ongoing trade studies concerning the use of the primary mirror actuators will help to allocate the amount of throw needed for correction of tacking errors, atmospheric dispersion correction, thermal expansion and of the gravitational flexure of the space frame.

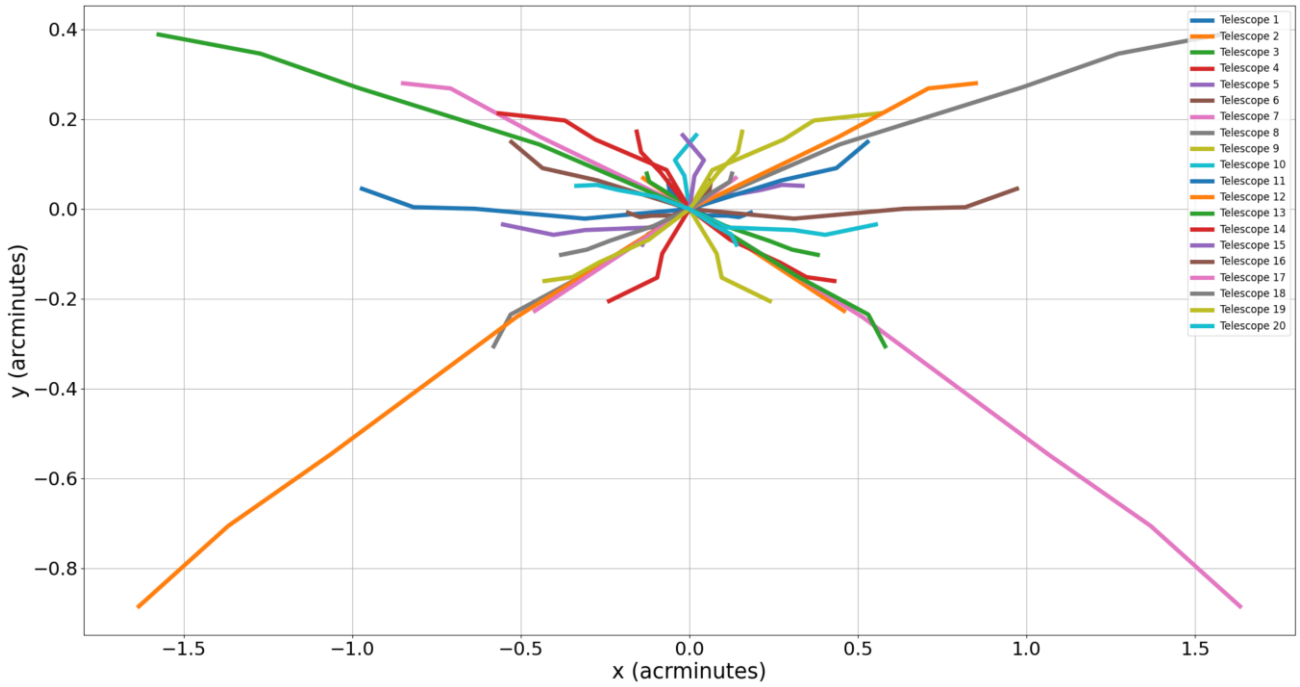

Figure 8: Pre-correction star image motion for all 20 unit telescopes when slewing in altitude from 0 - 90 degrees.

2.5 Dynamic Analysis of Tracking Mount

The dynamic performance of the tracking mount is important to quantify as it operates with no dome, directly subject to wind. Planned active image stabilization, provided through rapid translation of a lens element in the prime focus corrector, will provide correction for vibration amplitudes up several arcseconds at frequencies up to 20 Hz. Thus, structural vibration amplitudes of the space frame resulting from wind buffeting should be held below this level to remain within the actively correctable range. We have used modal analysis of the space frame to determine the lowest resonant frequencies and mode shapes which will be most readily excited by the wind. For the analysis of the tracking mount, the telescope was pointed at the horizon with the drive locked. We assigned an estimated torsional stiffness of 20 x 10^6 Nm/rad to the elevation axis based on testing of a smaller scale slewing drives. The lowest modes, which will have the largest effects on pointing, are listed in Table 1.

Table 2: Lowest frequency modes for the LFAST Mount.

Mode and Frequency	Notes on Mode Shape
Mode 1: 4.64Hz	Diagonal twisting motion of tracking mount about the azimuth axis
Mode 2: 5.31Hz	Rocking of tracking mount about elevation axis
Mode 3: 6.71Hz	Twisting of tracking mount about optical axis (horizon pointing)
Mode 4: 6.79Hz	Twisting of tracking mount about azimuth axis
Mode 5: 10.88Hz	Swaying of tracking mount pier

Obtaining an accurate estimate of the vibration amplitudes for a given wind power spectral density would require complex and computationally expensive modeling of the tracking mount in a coupled fluid/solid model. For this early design, in lieu of such modeling, an estimation of the dynamic performance due to wind buffeting is achieved by scaling from the well characterized properties of the Atacama Large Millimeter Array (ALMA) antenna. The ALMA antenna has a 12m diameter dish driven in alt-az and operates with no dome in an environment similar to what we expect for LFAST and has similar lowest resonant frequencies. Research on the wind induced jitter of the prototype ALMA antennas has proven its performance to less than 1 arcsecond vibration amplitudes measured at windspeeds of 9 m/s at the Very Large Array site where testing occurred [4].

A simplified analysis of LFAST and ALMA compares the two telescopes when modeled as single DOF torsional mass spring systems of given moment of inertia and spring constant when subject to single frequency excitation at their respective resonant frequencies. The exciting force acting on the LFAST tracking mount was scaled down from that of ALMA's to be proportional with the reduced sail area of LFAST and its closer proximity with the ground. We calculated the torsional stiffness of the LFAST space frame using its measured rotational inertia and its resonant frequency from modal analysis. For the ALMA protype, we used its lowest resonant frequency associated with altitude axis nodding and a conservative estimate of the rotational inertia of the antenna about the altitude axis to approximate the stiffness. With the stiffness and rotational inertia of both systems characterized, we model the response amplitude of LFAST due to single frequency excitation at its natural frequency.

2.6 Results from Dynamic Analysis

From this simplified analysis, the LFAST tracking mount elevation axis was found to have roughly 9% the stiffness of the ALMA prototype antennas. With LFAST having 21% the wind exposed area of ALMA and half its total height, resulting in a 10.5% reduction in mean wind velocity, LFAST sees 17.4% of the force acting on the ALMA antenna from the same gust of wind. This assumes the drag coefficient and air density are identical for both. Considering the reduced stiffness and forces acting on LFAST, the vibration amplitudes resulting from single frequency excitation are approximated to be 1.9 times larger than that of ALMA. Using results published for the ALMA prototype antennas of ~0.6 arcseconds, a total vibration amplitude of ~1.2 arcseconds is estimated for LFAST. This is similar to the desired ~1 arcsecond and an indication that the current design is feasible for use in open air environments similar to the VLA test site in New Mexico. Further investigation into wind induced jitter will employ the use of accelerometers and field testing of the first built LFAST tracking mount.

3. PRIMARY MIRROR SUPPORT

3.1 Design

The mirror support system is a whiffletree design with kinematic rod flexures to attach the whiffle tree components and the primary mirror, modeled on designs for the segments of telescopes like the TMT and ELT. The whiffletree components have centers of mass coincident with their respective centers of rotation ensuring that they remain balanced at all pointing altitudes and don't impart extraneous moments into the back of the mirrors. The use of rod flexures in the axial support system requires that the assembly of the whiffletree be precise, so as to not preload the flexure rods. However, these flexure rods can be made cheaply in large quantity and their behavior is predictable. We use alloy pucks with a similar coefficient

of thermal expansion to the primary mirror to attach the rods to the back of the primary mirrors. Lateral support comes from a centrally mounted spherical bearing which rides on a lateral support shaft in lieu of a central diaphragm type support. While this support is non kinematic, it is less sensitive to assembly errors resulting in a push/pull in the center of the primary mirror. Its performance will be explored in the prototype unit telescope. Tangential constraints on the primary mirror will make use of the bonded pucks, used for axial support, and react against the supporting subframe of the mirror cell. An exploded view of the primary mirror, whiffle tree, linear actuators and supporting subframe are shown in Figure 9.

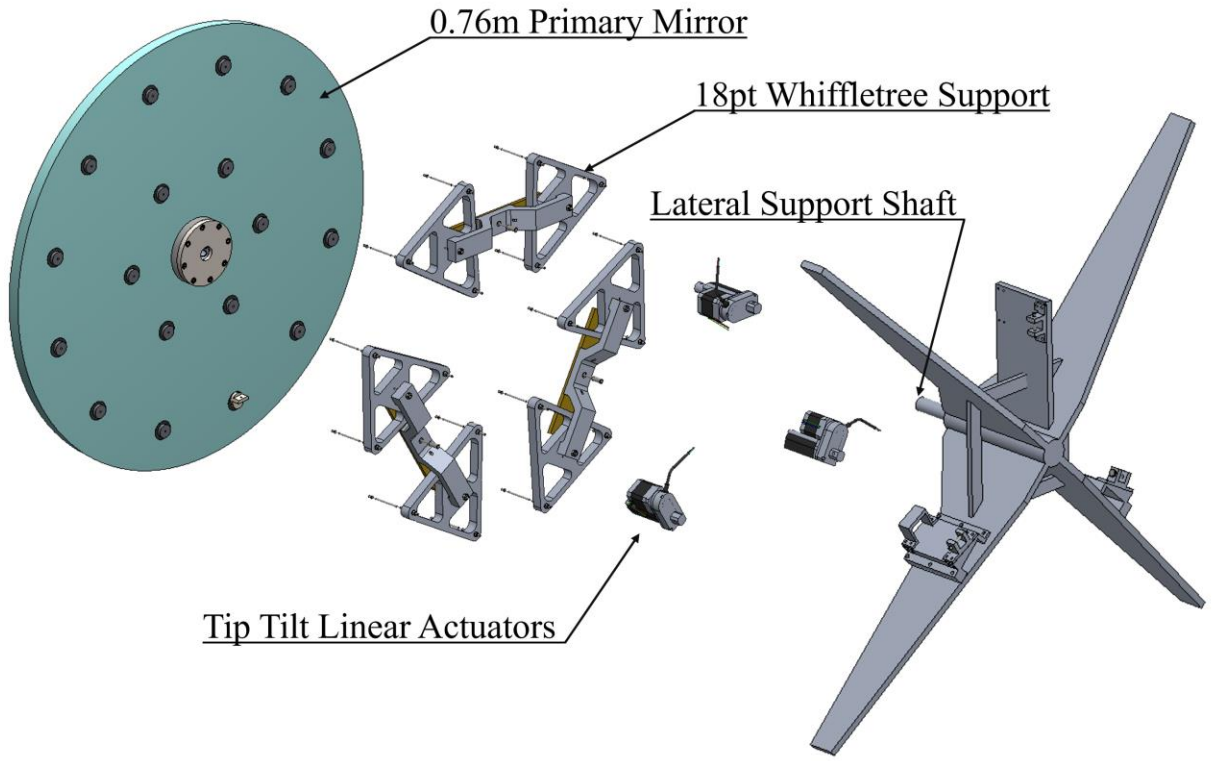

Figure 9: LFAST primary mirror, axial support whiffletree, tip/tilt linear actuators, lateral support system and sub frame assemblies.

3.2 Finite Element Modeling

Initial design of the whiffletree was done using a closed form solution for plates on point supports [5]. This revealed that a support topology of 18points provided an approximate ~10nm RMS surface error and is well suited to this application. On this basis, a finite element model of the meniscus primary mirror was made. Parameterized sketches defining the locations of the support points were driven by an optimization routine minimizing the RMS surface error. Over several iterations with this model the optimum support topology was computed. Then, a more complete model was developed to capture the interactions between the flexure rods connecting the whiffletree components together and the flexure rods connecting the whiffletree to the primary mirror. This model aids in determining the influence various assembly related errors have on the final surface RMS and informs the component tolerances of the design that are critical to good performance. This updated model, shown in Figure 10, attempts to capture this detail. Each of the flexure rods in the whiffletree are modeled as torsional springs, with the flexure rods connecting the mirror to the whiffletree modeled with beam elements.

Standard Earth Gravity [C]
- Applied to plate Body
- 9.8066m/s^2

XYZ-Displacement [B]:
- Applied to center of each of the 3 balances
- X Component – 0
- Y Component – 0
- Z Component – 0

Remote Displacement [A]:
- Applied to central hole
- X Coord – 0
- Y Coord – 0
- Z Coord – Variable (Starts at Mirror CG)
- X Component – 0
- Y Component – 0
- Z Component – FREE
- X Rotation – FREE
- Y Rotation – FREE
- Z Rotation – FREE

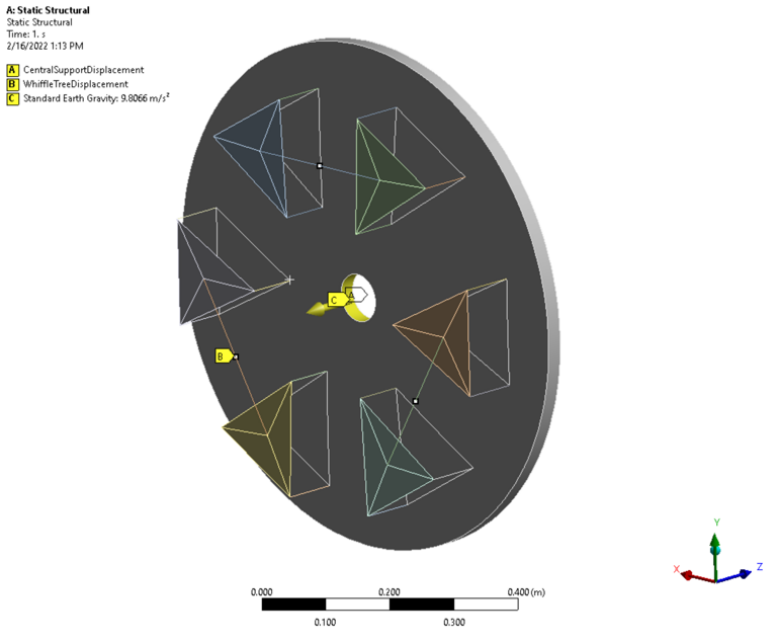

Figure 10: Whiffletree analysis model to observe effects of error in manufacture and assembly.

3.3 Static Analysis of Primary Mirror Whiffletree

Optimization of the primary mirror found that axial support deformations can be held to 9.6nm RMS using an 18point system resulting in a 1% decrease of encircled energy at the 17um optical fiber. Contours of surface deflection are shown in Figure 11. A central obscuration of 0.127m and the final 0.0254m of the edge of the primary were excluded from the analysis as these areas of the aperture are not reflective.

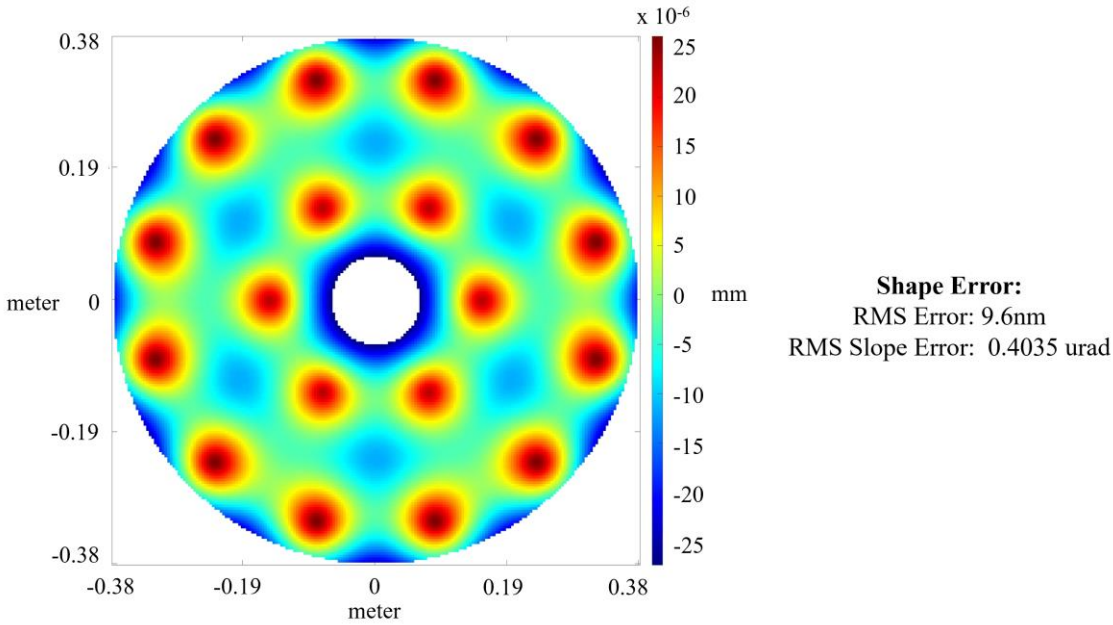

Figure 11: Contour map of the deformed primary mirror surface on the optimized 18 point whiffle tree.

The lateral support of the primary mirror on the central spherical bearing was optimized to minimize surface RMS using the placement of the spherical bearings with respect to the center of gravity of the mirror. The optimum placement is with the bearing 6mm behind the mirrors center of gravity giving an RMS surface error of 71nm. Shown in Figure 12 is the surface error when pointing to 30 degrees above the horizon, yielding an error of 59nm RMS. Ray trace analysis of the image reflected from this surface indicates a 4% reduction in encircled energy at the 17um optical fiber. As error budgets associated with the optical performance become more granular, this aspect of the mirror support will likely need to be improved by counterweighting the whiffle tree components.

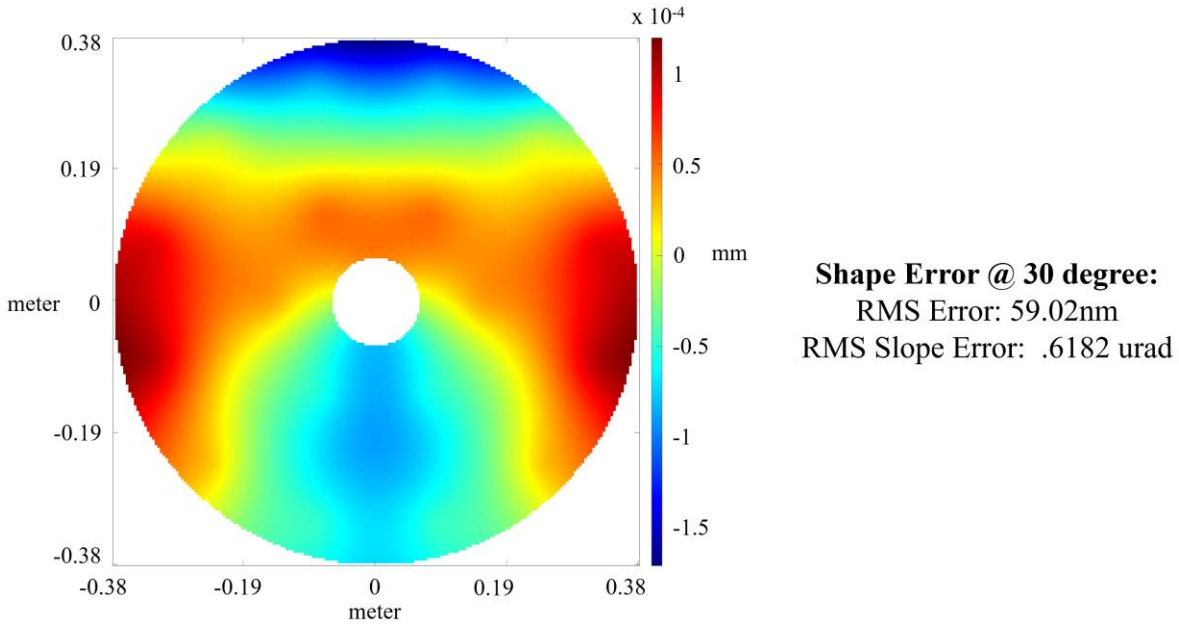

Figure 12: Surface error of the 0.76m primary mirror with central lateral support and 18pt whiffletree axial support when pointing to 30 degrees.

4. CONCLUSIONS

The optomechanical designs presented here of the unit telescopes and a novel open-air tracking mount for LFAST indicate that seeing-limited imaging performance should be achievable. The mount design is chosen with a central pier mounted alt-az drive between the 20 supported 0.76 m telescopes to minimize differential flexure, to better than an arcminute over a range of elevations. Given centering of star images by active tip tilt of the primary mirrors, residual image aberrations due to flexure of the mount space frame are minimal, decreasing the encircled energy in the fiber cores by a maximum 0.63 %, for altitudes from 30 to 90 degrees. Vibration of the tracking mount resulting from wind buffeting was estimated to have amplitudes of order 1 arcsecond at 5 Hz, to be corrected by active image stabilization by the prime focus corrector. Through the use of a guide camera on each unit telescope, residual errors in the telescope's alignment and motion from wind jitter are captured and fed back in closed loop to keep the star images centered on the 17um fibers. A design for a passive whiffletree support for the primary mirrors was optimized and shown to reduce the energy encircled within the 17um fiber core by only 1% at when zenith pointing and by 4% when point at 30 degrees in elevation

5. ACKNOWLADGMENTS

This research was funded by the generosity of Eric and Wendy Schmidt, by recommendation of the Schmidt Futures program. Thanks to Ruben Dominguez who contributed towards the design of the primary mirror support structure and Eric Williams who aided in the conceptual development of the whiffletree and for his insights into error analysis.

REFERENCES

[1] Angel, J. et al., “The Large Fiber Array Spectroscopic Telescope,” These proceedings, (2022).

[2] Bender, C. et al., “The Large Fiber Array Spectroscopic Telescope: Fiber feed and spectrometer conceptual design,” These proceedings, (2022).

[3] Snel, Ralph C, Jeffrey G Mangum, and Jacob W.M Baars., "Study of the Dynamics of Large Reflector Antennas with Accelerometers," IEEE Antennas & Propagation Magazine 49.4, 84-101. (2007).

[4] Berkson, J. et al., “The Large Fiber Array Spectroscopic Telescope: Optical Design of the Unit Telescope,” These proceedings, (2022).

[5] Nelson, Jerry E, Jacob Lubliner, and Terry S Mast., “Telescope Mirror Supports: Plate Deflections On Point Supports,” 332, 212-28. (1982)